

The Baryonic Tully-Fisher Relation of HI-bearing Low Surface Brightness Galaxies Implies Their Formation Mechanism

Zichen Hua^{1,2}, Yu Rong^{1,2*}, Huijie Hu^{3,4}

¹Department of Astronomy, University of Science and Technology of China, Hefei 230026, China

²School of Astronomy and Space Sciences, University of Science and Technology of China, Hefei 230026, China

³University of Chinese Academy of Sciences, Beijing 100049, China

⁴National Astronomical Observatories, Chinese Academy of Sciences, Beijing 100012, China

Accepted XXX. Received YYY; in original form ZZZ

ABSTRACT

We investigate the baryonic Tully-Fisher relation in low surface brightness galaxies selected from the Arecibo Legacy Fast ALFA survey. We find that the HI-bearing low surface brightness galaxies still follow the baryonic Tully-Fisher relation of typical late-type galaxies, with a slope of approximately 4 in the baryonic mass versus rotational velocity diagram on the logarithmic scale, i.e., $M_b \propto v_{\text{rot}}^4$. Our findings suggest that the matter distributions in low surface brightness galaxies may resemble that of general late-type galaxies, and hint that low surface brightness galaxies may not originate from dark matter halos of low densities or stronger/weaker feedback processes, but may emerge from dark matter halos with high spin values.

Key words: galaxies: kinematics and dynamics – galaxies: formation – galaxies: evolution

1 INTRODUCTION

Low surface brightness galaxies (LSBGs) constitute a special population of galaxies with central surface brightness at least one magnitude fainter than that of the sky background (i.e., B -band surface brightness $\geq 22.5 \text{ mag} \cdot \text{arcsec}^{-2}$; Impey & Bothun 1997; Bothun et al. 1997). In the fields, LSBGs have been observed to exhibit higher HI fractions (Du et al. 2015; He et al. 2020), lower star formation rates (Wyder et al. 2009; Rong et al. 2020b), and low metallicities (Kuzio de Naray et al. 2004). Also, LSBGs tend to appear in low-density environments (Pérez-Montaño & Cervantes Sodi 2019; Mo et al. 1994; Galaz et al. 2011).

The formation and evolution mechanisms of LSBGs, which play a crucial role in refining our current models of galaxy formation and evolution, have gathered much attention ever since their initial detection. Early investigations often regarded LSBGs as galaxies formed in low-density dark matter halos (Dekel & Silk 1986; McGaugh 1992; Mo et al. 1994). However, more recent studies have presented more alternative scenarios. One of the most classical theories of the formation mechanism of LSBGs is that they are galaxies hosted in dark matter halos belonging to the high-spin tail of the spin distribution. In theoretical works and simulations, the halos of LSBGs are found to have higher spin parameters compared with high surface brightness galaxies, regardless of whether they are relatively massive (Mo et al. 1998; Kim & Lee 2013; Kulier et al. 2020; Pérez-Montaño et al. 2022), or belong to ultra-diffuse galaxies (UDGs, Rong et al. 2017; Amorisco & Loeb 2016; Rong et al. 2024) – a specific subset of LSBGs of smaller masses. Additionally, some studies suggest that low-mass LSBGs may represent failed L^* galaxies (van Dokkum

et al. 2015a,b), or originate from early co-planar mergers (Wright et al. 2021) or stellar feedback processes (Chan et al. 2018; Di Cintio et al. 2019), or birth during tidal interactions (Rong et al. 2020a; Carleton et al. 2019), or form through multiple pathways (Papastergis et al. 2017). High-mass LSBGs, alternatively, may form through mergers (Saburova et al. 2018; Di Cintio et al. 2019; Zhu et al. 2023), two-stage process with external gas accretions (Saburova et al. 2021), or dynamical evolution driven by bars (Noguchi 2001).

Nevertheless, despite extensive efforts, our present comprehension of the formation and evolution of LSBGs is still limited. One of the key reasons is that studies on the mass distributions and baryonic fractions in LSBGs have not achieved a consensus, and a comprehensive scenario has not been established to constrain the current formation and evolution models of LSBGs. Many studies have shown that the dynamics of LSBGs may be dominated by dark matter (e.g. de Blok & McGaugh 1997; Mowla et al. 2017), yet UDGs may exhibit a deficiency in dark matter content (e.g. van Dokkum et al. 2018; Mancera Piña et al. 2019). As for the stellar-to-halo mass relation ($M_* - M_{\text{halo}}$), while Prole et al. (2019) propose that LSBGs form a continuous extension of typical dwarfs in the $M_* - M_{\text{halo}}$ diagram, other studies reveal significant deviations for UDGs from the typical $M_* - M_{\text{halo}}$ relation (e.g. van Dokkum et al. 2018). Additionally, some giant LSBGs appear to be dominated by baryons at their central regions, akin to the high surface brightness galaxy (HSBG) counterparts (Lelli et al. 2010); the stellar-to-halo mass relation of the giant LSBGs and HSBGs also exhibits a similarity. All of these confusing signs of diversity in matter distribution among LSBGs could offer valuable insights into their varied formation and evolution pathways. Consequently, a comprehensive understanding of the matter distributions in LSBGs is essential for refining our current models of galaxy formation and evolution.

* Corresponding author; E-mail: rongyua@ustc.edu.cn

The baryonic Tully-Fisher relation (BTFR) is a correlation between the rotational velocity, v_{rot} , and the baryonic mass, M_{b} , of galaxies. Over the past two decades, many studies have shown that late-type galaxies and dwarf galaxies consistently adhere to a power-law form of BTFR, despite their wide ranges of baryonic mass, luminosity, and size. BTFR could be written as,

$$M_{\text{b}} \propto v_{\text{rot}}^{\beta}, \quad (1)$$

where the logarithmic slope, β , typically falls within a range from 3 to 4 (e.g. [McGaugh et al. 2000](#); [Begum et al. 2008](#); [Papastergis et al. 2016](#); [Lelli et al. 2016b](#); [Sales et al. 2017](#); [Goddy et al. 2021](#)). Notably, some studies have also discovered that early-type galaxies may also follow the BTFR of late-type galaxies ([den Heijer et al. 2015](#); [Serra et al. 2012](#)).

In the context of Λ CDM paradigm, the presence of BTFR is considered as a correlation between the virial velocity of the dark matter halo and the baryonic mass enclosed within that halo ([McGaugh 2012](#); [Mo et al. 1998](#)). Thus, it can serve as a valuable tool to probe the distribution of baryonic matter and dark matter within galaxies. Furthermore, simulations have highlighted the significance of feedback processes in shaping the observed BTFR (e.g. [Governato et al. 2010](#); [Piontek & Steinmetz 2011](#); [Dutton 2012](#)), suggesting that investigating the BTFR can serve as a valuable means to constrain the feedback mechanisms at work within galaxies. Additionally, BTFR is highly related to other dynamical relationships such as the radial acceleration relation (e.g. [McGaugh et al. 2016](#); [Lelli et al. 2017](#)). Exploring the BTFR could also provide insights into new gravitational theories, as a BTFR with $\beta = 4$ is well predicted by the Modified Newtonian Dynamics (MOND, [Milgrom 1983](#)). Given its multifaceted implications, the BTFR remains one of the most extensively studied dynamical relations in astrophysics.

As anticipated, recent studies examining the BTFR of LSBGs also show some potential signs of tension. The previous studies of, for instance, [Lelli et al. \(2016b\)](#) (see also [Zwaan et al. 1995](#)), have explored that the residuals of BTFR do not change with galactic surface brightness, while some of the recent investigations ([Hu et al. 2023](#); [Karunakaran et al. 2020](#); [Rong et al. 2024](#)) reveal that UDGs may significantly deviate from the BTFR of typical late-type galaxies. Therefore, a thorough and meticulous examination of the BTFR for LSBGs becomes essential. Such an analysis may not only indicate whether the matter distribution within LSBGs aligns with that of typical late-type and dwarf galaxies, but also provide valuable constraints on the formation mechanisms of LSBGs.

In this work, we will first introduce our sample selection in Section 2, and then describe our methods for calculating M_{b} and v_{rot} in Section 3. We will then present our results in Section 4, and finally discuss the potential selection biases, the radial acceleration relation, and the possible formation mechanism of LSBGs in Section 5. The summary is in Section 6.

2 SAMPLE SELECTION

The Arecibo Legacy Fast ALFA survey (ALFALFA) is a wide-area blind HI survey aimed at searching for HI-bearing objects in the extragalactic neighbourhood. [Haynes et al. \(2011\)](#) matched the HI sources in the ALFALFA α .40 catalogue with the optical catalogue of the Sloan Digital Sky Survey (SDSS) Data Release 7 (DR7), and obtained the ALFALFA-SDSS α .40 cross-matched catalogue. Based on this catalogue, [Du et al. \(2015\)](#) and [He et al. \(2020\)](#) have done photometry for each galaxy in this catalogue, and selected a sample of LSBGs with the B -band apparent central surface brightness between

$22.5 < \mu_{0B} < 27.64$ mag/arcsec². In this work, we use this LSBG sample as our parent sample.

From the parent sample, we first remove LSBGs with g -band apparent axis ratios $b/a > 0.72$, approximately corresponding to the threshold of inclination angles of $i \lesssim 45^\circ$, because that the face-on galaxies may introduce large uncertainties in the measurements of the rotation velocities (see equation (10)). We then exclude LSBGs with low HI spectral signal-to-noise ratios $\text{SNR} < 10$, and visually remove LSBGs with suspicious HI spectra.

Due to the bad spatial resolution of ALFALFA (being $3.8' \times 3.3'$; [Durbala et al. 2020](#)), if a galaxy has a close companion galaxy, its HI spectrum may be contaminated by the companion. To eliminate this possibility, we remove the sample galaxies with neighbouring galaxies within the projected radii of $3.8'$ (i.e., approximately the beam size of Arecibo) and radial velocity differences of $\Delta v < 500$ km/s. The redshift of a LSBG is estimated from the central velocity of its HI spectrum, while the redshift of the neighbouring galaxies comes from the SpecObj and Photoz databases of SDSS. Finally, 204 LSBGs are left in our sample.

We also calculate the kurtosis coefficients, k_4 , of the HI spectra ([Papastergis et al. 2016](#); [El-Badry et al. 2018](#)) for our sample galaxies, as

$$k_4 = M_4 / (\sigma^2)^2 - 3, \quad (2)$$

where M_4 and σ^2 are calculated as,

$$M_4 = \int_{v_{\text{min}}}^{v_{\text{max}}} (v - \bar{v})^4 F(v) dv / \int_{v_{\text{min}}}^{v_{\text{max}}} F(v) dv, \quad (3)$$

$$\sigma^2 = \int_{v_{\text{min}}}^{v_{\text{max}}} (v - \bar{v})^2 F(v) dv / \int_{v_{\text{min}}}^{v_{\text{max}}} F(v) dv. \quad (4)$$

In equations (3) and (4), v and $F(v)$ represent the frequency and the flux density, respectively, and \bar{v} is defined as,

$$\bar{v} = \int_{v_{\text{min}}}^{v_{\text{max}}} v F(v) dv / \int_{v_{\text{min}}}^{v_{\text{max}}} F(v) dv. \quad (5)$$

Here, v_{min} and v_{max} correspond to the minimal and maximum frequencies between which W_{20} (see Section 3 for the definition of W_{20}) is measured, respectively. The coefficient k_4 quantifies the ‘‘peakiness’’ of a spectrum and thus can indicate whether a spectrum is single-peaked or double-horned. The single-peaked galaxies may have kinematics strongly influenced by velocity dispersion ([El-Badry et al. 2018](#)), or HI disks that are not extended enough to trace the flat part of the rotation curve ([Papastergis et al. 2016](#)). As a consequence, their HI-widths might not represent their rotation velocities ([McGaugh 2012](#); [Verheijen 1997](#)). Therefore, we perform a cut at the HI spectrum, $k_4 < -1$, in order to remove the single-peaked galaxies.

The final sample contains 124 high-quality LSBGs with double-horned HI lines, ensuring the most reliable results. For comparison, 210 high surface brightness galaxies (HSBGs, $\mu_{0B} < 22.5$ mag) with double-horned HI lines are also selected from the α .40 catalog as the counterparts.

3 METHOD

We study the BTFRs of LSBGs and HSBGs by directly estimating the baryonic masses, M_{b} , and rotation velocities, v_{rot} , of the galaxies in the two samples.

The baryonic mass of a galaxy in our samples is mainly composed of the mass of stars and the mass of cold gas. The stellar mass M_* can be estimated with the galaxy luminosity in the $W1$ -band (denoted as L_{W1}) from the Wide-field Infrared Survey Explorer ([Wright et al.](#)

2010), using the method proposed by [McGaugh & Schombert \(2015\)](#), as

$$M_*/M_\odot = 0.45L_{W1}/L_\odot. \quad (6)$$

As for the mass of the cold gas, M_g , we estimate it by adding up the masses of HI and helium,

$$M_g = 1.33M_{\text{HI}}, \quad (7)$$

where M_{HI} is the HI mass. Equation (7) will certainly underestimate the mass of the gas since it neglects the mass of the molecular gas and hot ionized gas. However, the molecular gas fraction in the total gas component is low and thus negligible ([McGaugh 2012](#)). Also, the hot ionized gas usually resides outside the HI disk where our rotational velocity is measured ([Dutton 2012](#)), so it can be neglected. Therefore, approximately we estimate the baryonic mass of a galaxy as,

$$M_b = M_* + M_g. \quad (8)$$

For the rotation velocity, we estimate it using the 20% peak width of a HI spectrum (W_{20} ; [Guo et al. 2020](#); [Hu et al. 2023](#); [Rong et al. 2024](#)), as,

$$v_{\text{rot}} = \frac{W_{20}}{2 \sin i}, \quad (9)$$

where i is the inclination angle. W_{20} employed in equation (9) has been corrected for instrumental broadening and redshift ([Guo et al. 2020](#); [Kent et al. 2008](#)). In equation (9), we assume an alignment between the inclination angle of the stellar disk and HI disk in a galaxy, and then use the inclination angle of the stellar disk to estimate the rotation velocity. The inclination is estimated from the apparent axis ratio, as (e.g. [Guo et al. 2020](#); [Hu et al. 2023](#); [Du et al. 2019](#); [Rong et al. 2024](#); [Begum et al. 2008](#)),

$$\sin i = \sqrt{\frac{1 - (b/a)^2}{1 - q_0^2}}, \quad (10)$$

where q_0 denotes the intrinsic axis ratio seen edge-on. We take $q_0 = 0.2$, which is commonly used in the previous studies (e.g. [Du et al. 2019](#); [Guo et al. 2020](#); [Giovanelli et al. 1997](#); [Tully et al. 2009](#)). For those edge-on galaxies with g -band $b/a \leq 0.2$, we set $\sin i = 1$. Considering that the stellar disk and gas disk in galaxies may not be perfectly co-planar and often exhibit a small inclination difference of $\delta i < 20^\circ$ (e.g. [Gault et al. 2021](#)), we assume that the misalignment angle between the gas disk and the stellar disk, δi , follows a Gaussian distribution centred at 0° with a standard deviation of $\sigma = 20^\circ$. We treat $\sigma = 20^\circ$ as the uncertainty associated with i in our study.

4 RESULTS

In Figure 1, we observe that the distributions of the LSBGs and HSBGs exhibit no significant deviation in the $v_{\text{rot}} - M_b$ diagram. Subsequently, we impose a power-law equation,

$$\log(M_b) = \alpha + \beta \log(v_{\text{rot}}), \quad (11)$$

where α and β are both free parameters, to fit the BTFRs of the HSBGs and LSBGs, respectively. The best-fitting parameters of the BTFR of HSBGs are $\alpha_{\text{HSBG}} = 1.83 \pm 0.51$ and $\beta_{\text{HSBG}} = 3.91 \pm 0.24$, while the best-fitting parameters of LSBGs are $\alpha_{\text{LSBG}} = -1.45 \pm 1.49$ and $\beta_{\text{LSBG}} = 5.67 \pm 0.78$.

We further split LSBGs and HSBGs into the different $\log v_{\text{rot}}$ bins. Within each bin, we calculate the median value of $\log M_b$ and the corresponding 1σ standard deviation for both samples. As shown in

Figure 1, the binned points of LSBGs (depicted by the blue squares), as well as the binned points of HSBGs (depicted as the black squares), comfortably lie within the 1σ uncertainty region of the tightest BTFR of typical late-type galaxies reported by [Lelli et al. \(2019\)](#) (the red-solid line and the red-shaded region denote the best-fitting BTFR of typical late-type galaxies and its 1σ uncertainty, respectively, as shown in Fig. 1), with $\beta \simeq 3.85 \pm 0.09$.

Therefore, we conclude that the BTFRs of LSBGs and HSBGs show no significant deviation. Both galaxy samples follow the BTFR of typical late-type galaxies, with a BTFR slope of approximately 4.

5 DISCUSSION

5.1 Selection biases

In our study, the SNR threshold used to select the LSBG and HSBG samples may exclude some galaxies with similar HI masses but wider HI line widths from our parent sample, which might potentially introduce deviations in the slope of BTFR. To investigate the possible selection effects, we adjust the SNR threshold by increasing it from 10 to 15, or 20.

We find that, for HSBGs, the best-fitting β of their BTFR changes to 4.05 ± 0.21 for $\text{SNR} > 15$, and 4.05 ± 0.26 for $\text{SNR} > 20$, still in good agreement with the best-fitting β value for $\text{SNR} > 10$. For LSBGs, the best-fitting β becomes $\beta \sim 6.04 \pm 0.66$ ($\text{SNR} > 15$) and $\sim 6.13 \pm 0.82$ ($\text{SNR} > 20$), which is also similar to the $\beta \sim 5.67 \pm 0.78$ when applying the selection criterion of $\text{SNR} > 10$, considering the large uncertainties of the β values.

Additionally, the binned points of LSBGs and HSBGs within the different $\log v_{\text{rot}}$ for the different SNR thresholds are always located within the 1σ uncertainty region of the BTFR of typical late-type galaxies. Consequently, we conclude that, for both of LSBG and HSBG samples, the selection effect introduced by the SNR threshold is negligible.

5.2 The radial acceleration relation

Apart from BTFR, recently, a series of studies ([McGaugh et al. 2016](#); [Lelli et al. 2017](#); [Li et al. 2018](#); [Richards et al. 2018](#); [Rong et al. 2018](#); [Chae et al. 2020](#)) have revealed another tight correlation known as the radial acceleration relation (RAR). RAR indicates that the acceleration g_{bar} produced by the baryonic mass and the acceleration g_{obs} produced by the dynamical mass at any radius in many types of galaxies consistently follow a correlation of

$$g_{\text{obs}} = \frac{g_{\text{bar}}}{1 - e^{-\sqrt{g_{\text{bar}}/a_0}}}, \quad (12)$$

where $a_0 \simeq (1.20 \pm 0.02 \pm 0.24) \times 10^{-10} \text{ m/s}^2$ ([McGaugh et al. 2016](#); [Lelli et al. 2017](#)) is constant. In the Λ CDM paradigm, RAR plausibly suggests a universally established link between the mass distributions of baryonic matter and dark matter in galaxies.

We estimate g_{obs} and g_{bar} of each galaxy at its HI-radius (R_{HI}) using the following equations,

$$g_{\text{obs}} = \frac{v_{\text{rot}}^2}{R_{\text{HI}}}, \quad (13)$$

$$g_{\text{bar}} = x_* \frac{GM_*}{R_{\text{HI}}^2} + x_g \frac{GM_g}{R_{\text{HI}}^2}, \quad (14)$$

where G is the gravitational constant. x_* and x_g in equation (14) are correction factors assuming that the cold gas and stars are distributed

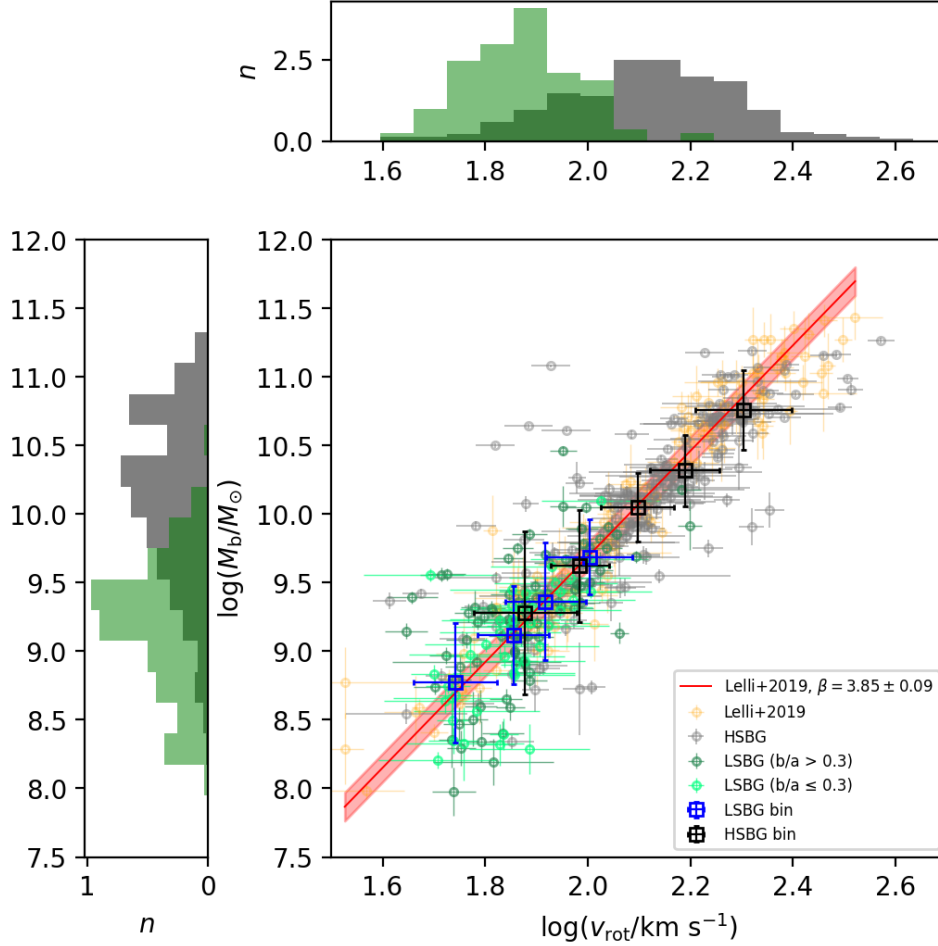


Figure 1. $v_{\text{rot}} - M_{\text{b}}$ diagram for our samples. The green circles represent LSBGs, while the grey circles represent HSBGs, and the orange circles are SPARC galaxies from Lelli et al. (2019). All the error bars denote 1σ uncertainties. The blue squares represent the median values of LSBGs while the black squares represent that of HSBGs. The red-solid line is the tightest BTFR reported by Lelli et al. (2019). The red-shaded area is the 1σ intrinsic scatter of the red-solid line, which is considered as the 1σ uncertainty of the tightest BTFR. The sub-panels display the number-density distribution of LSBGs (green histograms) and HSBGs (grey histograms).

in two razor-thin disks, respectively. They are calculated as (Freeman 1970),

$$x_* = I_0\left(\frac{R_{\text{HI}}}{2R_{d,*}}\right)K_0\left(\frac{R_{\text{HI}}}{2R_{d,*}}\right) - I_1\left(\frac{R_{\text{HI}}}{2R_{d,*}}\right)K_1\left(\frac{R_{\text{HI}}}{2R_{d,*}}\right), \quad (15)$$

$$x_g = I_0\left(\frac{R_{\text{HI}}}{2R_{d,g}}\right)K_0\left(\frac{R_{\text{HI}}}{2R_{d,g}}\right) - I_1\left(\frac{R_{\text{HI}}}{2R_{d,g}}\right)K_1\left(\frac{R_{\text{HI}}}{2R_{d,g}}\right), \quad (16)$$

where I_n and K_n are the modified Bessel functions of the first and second kind, respectively; $R_{d,*}$ and $R_{g,*}$ involved are the scale lengths of the stellar and HI disks which can be derived by using the same method described in the work of Rong et al. (2024).

R_{HI} corresponds to the outer region of a galaxy where the surface density of HI equals $1 M_{\odot}/\text{pc}^2$ (Broeils & Rhee 1997). R_{HI} can be estimated from the following tight correlation between HI mass and R_{HI} , which has been observed in various types of galaxies including LSBGs (Wang et al. 2016; Gault et al. 2021; Lutz et al. 2018),

$$\log\left(\frac{2R_{\text{HI}}}{\text{kpc}}\right) = (0.506 \pm 0.003) \log\left(\frac{M_{\text{HI}}}{M_{\odot}}\right) - (3.293 \pm 0.009). \quad (17)$$

In Figure 2, at R_{HI} , both our sample LSBGs and HSBGs follow the universal RAR (McGaugh et al. 2016; Lelli et al. 2017, as illustrated

by the red components in Fig. 2). The similarity of RARs between LSBG and HSBGs may suggest comparable mass distributions in the two galaxy samples.

It is worth noting that, at a large radius of a galaxy where $g_{\text{bar}} \ll a_0$, such as R_{HI} , the RAR described by equation (12) is actually equivalent to the BTFR with $\beta = 4$ (Lelli et al. 2017).

5.3 Implications on the formation mechanisms of LSBGs

Previous theoretical studies posit that LSBGs may form in low-density dark matter halos (e.g. Dekel & Silk 1986; McGaugh 1992). However, this model predicts a significant difference in the BTFRs between LSBGs and HSBGs (McGaugh 2021), which contradicts our findings. Therefore, the formation model based on low-density dark matter halos may not refer to LSBGs.

Many observational studies also suggest that LSBGs might be dominated by dark matter compared with HSBGs (e.g. de Blok & McGaugh 1997). Therefore, we delve deeper into understanding the fraction of dark matter in LSBGs. Note that BTFR could be expressed

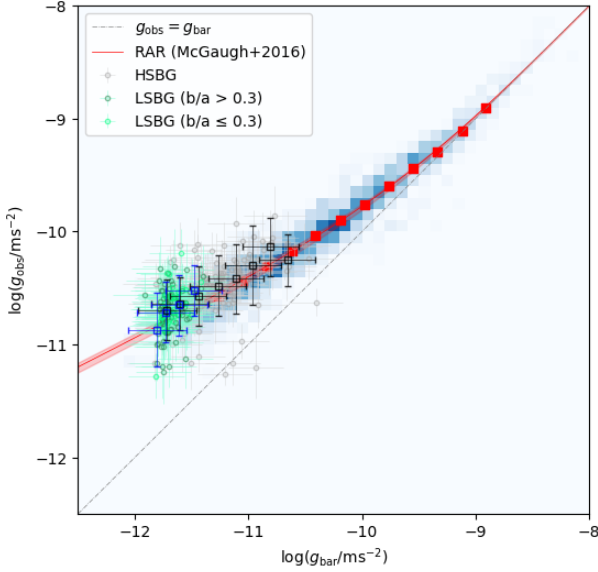


Figure 2. The RAR of our sample galaxies, overplotted by data from Lelli et al. (2016a). The circles and squares are the same as those in Figure 1. The red-solid line is the best-fitted RAR in previous studies (McGaugh et al. 2016; Lelli et al. 2017), and the grey-dot-dashed line is the identical line.

as ¹,

$$M_b \simeq \frac{f_b^2(R)}{G g_{\text{bar}}(R)} v_{\text{rot}}^4 \quad (18)$$

where R corresponds to a large radius in the outer region of a galaxy (such as R_{HI}), and

$$f_b(R) = \frac{M_b}{M_b + M_{\text{DM}}(R)}, \quad (19)$$

is the baryonic mass fraction within R , where $M_{\text{DM}}(R)$ denotes the dark matter mass enclosed within R . $g_{\text{bar}}(R)$ is the baryonic acceleration at R , which could be calculated with equation (14). Consequently, $f_b(R_{\text{HI}})$ of the LSBGs and HSBGs can be estimated with equation (18).

We examine the variation of $f_b(R_{\text{HI}})$ as a function of v_{rot} for both LSBGs and HSBGs. As shown in Fig. 3, in statistics, $f_b(R_{\text{HI}})$ increases with rising v_{rot} , with a slope of ~ 1.02 using a bisector fitting (Isobe et al. 1990). Since the dark matter halo mass of a galaxy is tightly related to v_{rot} , as $M_h \propto v_{\text{rot}}^3$ (Mo et al. 1998), the correlation between $f_b(R_{\text{HI}})$ and v_{rot} hints at a positive association between the baryonic mass fractions and dark matter halo masses for these galaxies (Ayromlou et al. 2023; Duffy et al. 2010). This correlation does not exceed our expectations, given that our galaxy samples are dominated by the low-mass galaxies. Halos with lower M_h have shallower potentials (Duffy et al. 2010), making it more difficult to prevent the galactic interstellar medium (ISM) against expulsion by the feedback processes in these shallower potentials, which leads to lower $f_b(R_{\text{HI}})$ (e.g. Bryan et al. 2013; Duffy et al. 2010).

Subsequently, in order to compare the $f_b(R_{\text{HI}})$ of the LSBG and HSBG samples with similar dark matter halo masses, we further focus on a specific v_{rot} bin defined by $\log v_{\text{rot}} \in [1.87, 2.05]$ (as depicted

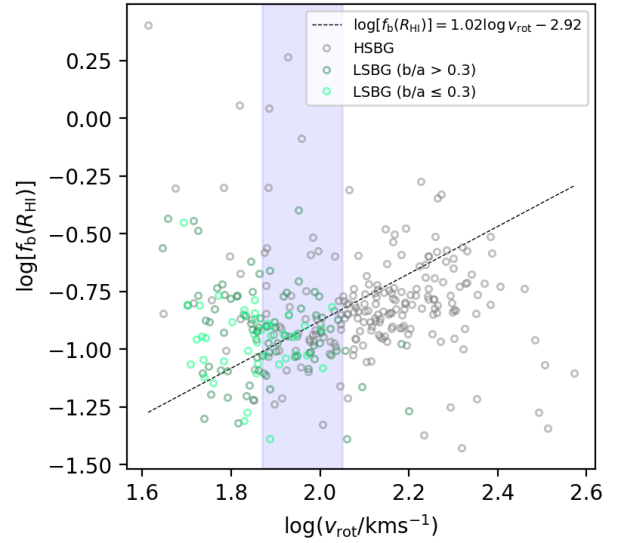


Figure 3. The $v_{\text{rot}} - f_b(R_{\text{HI}})$ relation of our sample galaxies. The circles are the same as those in Figure 1. The blue-shaded area represents the bin in which we perform Kuiper tests in Section 5.3. The black-dashed line is the best-fitted line for the data points.

by the blue-shaded region in Fig. 3). We have 52 LSBGs and 52 HSBGs in this small bin, exhibiting similar distributions of v_{rot} with median $\log v_{\text{rot}}$ values of 1.94 ± 0.05 (for LSBGs) and 1.97 ± 0.05 (for HSBGs). The Kuiper test between the distributions of v_{rot} of LSBGs and HSBGs in this small bin also gives a large p -value of 0.77, indicating no significant difference in v_{rot} . We then compare the $f_b(R_{\text{HI}})$ distributions of the LSBG and HSBG sample galaxies within this v_{rot} bin. The median values of the $f_b(R_{\text{HI}})$ distributions of LSBGs and HSBGs are -0.94 ± 0.15 and -0.91 ± 0.30 , respectively; the Kuiper test for the two $f_b(R_{\text{HI}})$ distributions also yields a large p -value of 0.34.

Therefore, we note that, for the LSBGs and HSBGs with similar halo masses, their baryonic fractions are also comparable. LSBGs are not particularly dark matter dominated galaxies, compared with the HSBG counterparts. Furthermore, this result also plausibly suggests comparable feedback power among the LSBGs and HSBGs with similar halo masses (i.e., similar gravitational potentials). Consequently, we conclude that feedback may not be the primary driver of the different surface brightness between these HI-bearing galaxies. In other words, these HI-bearing LSBGs may not originate from stronger or weaker feedback.

Alternatively, our finding aligns with the simulation results where the LSBGs can be well reproduced by higher dark matter halo spins (Pérez-Montaño et al. 2022). Therefore, we conclude that our result may lend support to the theorem that LSBGs may originate from high-spin dark matter halos (Mo et al. 1998).

5.4 Implications on MOND

Except for the aforementioned formation models of LSBGs in the framework of Λ CDM, MOND may also offer a reasonable explanation for the BTFR and RAR of LSBGs (e.g. Milgrom 1983; Wittenburg et al. 2020).

As demonstrated in Section 4 and 5.2, both LSBGs and HSBGs adhere to a BTFR with a slope indistinguishable from 4, and may follow the same RAR as given by equation (12). These results adhere

¹ Equation (19) is from the lecture on Tully-Fisher relation; see also Aaronson et al. (1979) and Zwaan et al. (1995).

to the theoretical predictions by MOND (Milgrom 1983). Therefore, our result cannot exclude the MOND theory.

6 SUMMARY

Taking advantage of the ALFALFA HI survey data, we have selected the HI-bearing LSBGs and HSBGs, and estimated their baryonic masses M_b and rotation velocities v_{rot} . Our findings reveal that, statistically, the HI-bearing LSBGs and HSBGs also conform to the BTFR found in typical late-type galaxies as well as ordinary dwarf galaxies with slope of $\beta \sim 4$. These results hint that LSBGs may owe their properties to the high spins of their host dark matter halos, rather than the halo densities or feedback processes. Additionally, our findings do not rule out the Modified Newtonian Dynamics (MOND) theory.

Our findings conflict with the BTFR results of UDGs (Karunakaran et al. 2020; Hu et al. 2023; Rong et al. 2024). This is primarily because that our LSBG sample contains very few UDGs. Indeed, almost all of our LSBGs are classic LSBGs, rather than UDGs with extremely large effective radii. Therefore, we propose that UDGs may be a distinct galaxy population with different BTFR and mass distributions, compared with typical LSBGs. They may also have distinct formation mechanisms that warrant further investigations.

ACKNOWLEDGEMENTS

We sincerely thank Xufen Wu, Haochen Jiang, Jingshuo Yang, Shijiang Chen and Yu Chen for the inspiring discussions during this study. Y.R. acknowledges supports from the NSFC grant 12273037, and the CAS Pioneer Hundred Talents Program (Category B), as well as the USTC Research Funds of the Double First-Class Initiative (No. YD2030002013). H.H. is supported by the Fundamental Research Funds for the Central Universities, the CAS Project for Young Scientists in Basic Research Grant No. YSBR-062, the National SKA Program of China No. 2022SKA0110201, and the NSFC grant No. 12033008.

DATA AVAILABILITY

Data are available if requested.

REFERENCES

Aaronson M., Huchra J., Mould J., 1979, *ApJ*, **229**, 1
 Amorisco N. C., Loeb A., 2016, *MNRAS*, **459**, L51
 Ayromlou M., Nelson D., Pillepich A., 2023, *MNRAS*, **524**, 5391
 Begum A., Chengalur J. N., Karachentsev I. D., Sharina M. E., 2008, *MNRAS*, **386**, 138
 Bothun G., Impey C., McGaugh S., 1997, *PASP*, **109**, 745
 Broeils A. H., Rhee M. H., 1997, *A&A*, **324**, 877
 Bryan S. E., Kay S. T., Duffy A. R., Schaye J., Dalla Vecchia C., Booth C. M., 2013, *MNRAS*, **429**, 3316
 Carleton T., Errani R., Cooper M., Kaplinghat M., Peñarrubia J., Guo Y., 2019, *MNRAS*, **485**, 382
 Chae K.-H., Bernardi M., Domínguez Sánchez H., Sheth R. K., 2020, *ApJ*, **903**, L31
 Chan T. K., Kereš D., Wetzel A., Hopkins P. F., Faucher-Giguère C. A., El-Badry K., Garrison-Kimmel S., Boylan-Kolchin M., 2018, *MNRAS*, **478**, 906

Dekel A., Silk J., 1986, *ApJ*, **303**, 39
 Di Cintio A., Brook C. B., Macciò A. V., Dutton A. A., Cardona-Barrero S., 2019, *MNRAS*, **486**, 2535
 Du W., Wu H., Lam M. I., Zhu Y., Lei F., Zhou Z., 2015, *AJ*, **149**, 199
 Du W., Cheng C., Wu H., Zhu M., Wang Y., 2019, *MNRAS*, **483**, 1754
 Duffy A. R., Schaye J., Kay S. T., Dalla Vecchia C., Battye R. A., Booth C. M., 2010, *MNRAS*, **405**, 2161
 Durbala A., Finn R. A., Crone Odekon M., Haynes M. P., Koopmann R. A., O'Donoghue A. A., 2020, *AJ*, **160**, 271
 Dutton A. A., 2012, *MNRAS*, **424**, 3123
 El-Badry K., et al., 2018, *MNRAS*, **477**, 1536
 Freeman K. C., 1970, *ApJ*, **160**, 811
 Galaz G., Herrera-Camus R., Garcia-Lambas D., Padilla N., 2011, *ApJ*, **728**, 74
 Gault L., et al., 2021, *ApJ*, **909**, 19
 Giovanelli R., Haynes M. P., Herter T., Vogt N. P., Wegner G., Salzer J. J., da Costa L. N., Freudling W., 1997, *AJ*, **113**, 22
 Goddy J., Stark D., Masters K., 2021, in American Astronomical Society Meeting Abstracts. p. 148.09
 Governato F., et al., 2010, *Nature*, **463**, 203
 Guo Q., et al., 2020, *Nature Astronomy*, **4**, 246
 Haynes M. P., et al., 2011, *AJ*, **142**, 170
 He M., Wu H., Du W., Liu H.-y., Lei F.-j., Zhao P.-s., Zhang B.-q., 2020, *ApJS*, **248**, 33
 Hu H.-J., Guo Q., Zheng Z., Yang H., Tsai C.-W., Zhang H.-X., Zhang Z.-Y., 2023, *ApJ*, **947**, L9
 Impey C., Bothun G., 1997, *ARA&A*, **35**, 267
 Isobe T., Feigelson E. D., Akritas M. G., Babu G. J., 1990, *ApJ*, **364**, 104
 Karunakaran A., Spekkens K., Zaritsky D., Donnerstein R. L., Kadowaki J., Dey A., 2020, *ApJ*, **902**, 39
 Kent B. R., et al., 2008, *AJ*, **136**, 713
 Kim J.-h., Lee J., 2013, *MNRAS*, **432**, 1701
 Kulier A., Galaz G., Padilla N. D., Trayford J. W., 2020, *MNRAS*, **496**, 3996
 Kuzio de Naray R., McGaugh S. S., de Blok W. J. G., 2004, *MNRAS*, **355**, 887
 Lelli F., Fraternali F., Sancisi R., 2010, *A&A*, **516**, A11
 Lelli F., McGaugh S. S., Schombert J. M., 2016a, *AJ*, **152**, 157
 Lelli F., McGaugh S. S., Schombert J. M., 2016b, *ApJ*, **816**, L14
 Lelli F., McGaugh S. S., Schombert J. M., Pawłowski M. S., 2017, *ApJ*, **836**, 152
 Lelli F., McGaugh S. S., Schombert J. M., Desmond H., Katz H., 2019, *MNRAS*, **484**, 3267
 Li P., Lelli F., McGaugh S., Schombert J., 2018, *A&A*, **615**, A3
 Lutz K. A., et al., 2018, *MNRAS*, **476**, 3744
 Mancera Piña P. E., et al., 2019, *ApJ*, **883**, L33
 McGaugh S. S., 1992, PhD thesis, University of Michigan
 McGaugh S. S., 2012, *AJ*, **143**, 40
 McGaugh S. S., 2021, *Studies in History and Philosophy of Science*, **88**, 220
 McGaugh S. S., Schombert J. M., 2015, *ApJ*, **802**, 18
 McGaugh S. S., Schombert J. M., Bothun G. D., de Blok W. J. G., 2000, *ApJ*, **533**, L99
 McGaugh S. S., Lelli F., Schombert J. M., 2016, *Phys. Rev. Lett.*, **117**, 201101
 Milgrom M., 1983, *ApJ*, **270**, 371
 Mo H. J., McGaugh S. S., Bothun G. D., 1994, *MNRAS*, **267**, 129
 Mo H. J., Mao S., White S. D. M., 1998, *MNRAS*, **295**, 319
 Mowla L., van Dokkum P., Merritt A., Abraham R., Yagi M., Koda J., 2017, *ApJ*, **851**, 27
 Noguchi M., 2001, *MNRAS*, **328**, 353
 Papastergis E., Adams E. A. K., van der Hulst J. M., 2016, *A&A*, **593**, A39
 Papastergis E., Adams E., Romanowsky A., 2017, *Astronomy & Astrophysics*, **601**, L10
 Pérez-Montaño L. E., Cervantes Sodi B., 2019, *MNRAS*, **490**, 3772
 Pérez-Montaño L. E., Rodríguez-Gomez V., Cervantes Sodi B., Zhu Q., Pillepich A., Vogelsberger M., Hernquist L., 2022, *MNRAS*, **514**, 5840
 Piontek F., Steinmetz M., 2011, *MNRAS*, **410**, 2625
 Prole D. J., et al., 2019, *MNRAS*, **484**, 4865
 Richards E. E., et al., 2018, *MNRAS*, **476**, 5127

- Rong Y., Guo Q., Gao L., Liao S., Xie L., Puzia T. H., Sun S., Pan J., 2017, *MNRAS*, **470**, 4231
- Rong Y., Li H., Wang J., et al. 2018, *MNRAS*, **477**, 230
- Rong Y., Dong X.-Y., Puzia T. H., et al. 2020a, *ApJ*, **899**, 78
- Rong Y., Zhu K., Johnston E. J., Zhang H.-X., Cao T., Puzia T. H., Galaz G., 2020b, *ApJ*, **899**, L12
- Rong Y., Hu H., He M., Du W., Guo Q., Wang H.-Y., Zhang H.-X., Mo H., 2024, *arXiv e-prints*, p. [arXiv:2404.00555](https://arxiv.org/abs/2404.00555)
- Saburova A. S., Chilingarian I. V., Katkov I. Y., Egorov O. V., Kasparova A. V., Khoperskov S. A., Uklein R. I., Vozyakova O. V., 2018, *MNRAS*, **481**, 3534
- Saburova A. S., Chilingarian I. V., Kasparova A. V., Sil'chenko O. K., Grishin K. A., Katkov I. Y., Uklein R. I., 2021, *MNRAS*, **503**, 830
- Sales L. V., et al., 2017, *MNRAS*, **464**, 2419
- Serra P., et al., 2012, *MNRAS*, **422**, 1835
- Tully R. B., Rizzi L., Shaya E. J., Courtois H. M., Makarov D. I., Jacobs B. A., 2009, *AJ*, **138**, 323
- Verheijen M. A. W., 1997, PhD thesis, Univ. Groningen
- Wang J., Koribalski B. S., Serra P., van der Hulst T., Roychowdhury S., Kamphuis P., Chengalur J. N., 2016, *MNRAS*, **460**, 2143
- Wittenburg N., Kroupa P., Famaey B., 2020, *ApJ*, **890**, 173
- Wright E. L., et al., 2010, *AJ*, **140**, 1868
- Wright A. C., Tremmel M., Brooks A. M., Munshi F., Nagai D., Sharma R. S., Quinn T. R., 2021, *MNRAS*, **502**, 5370
- Wyder T. K., et al., 2009, *ApJ*, **696**, 1834
- Zhu Q., Pérez-Montaña L. E., Rodríguez-Gomez V., Cervantes Sodi B., Zjupa J., Marinacci F., Vogelsberger M., Hernquist L., 2023, *MNRAS*, **523**, 3991
- Zwaan M. A., van der Hulst J. M., de Blok W. J. G., McGaugh S. S., 1995, *MNRAS*, **273**, L35
- de Blok W. J. G., McGaugh S. S., 1997, *MNRAS*, **290**, 533
- den Heijer M., et al., 2015, *A&A*, **581**, A98
- van Dokkum P. G., Abraham R., Merritt A., Zhang J., Geha M., Conroy C., 2015a, *ApJ*, **798**, L45
- van Dokkum P. G., et al., 2015b, *ApJ*, **804**, L26
- van Dokkum P., et al., 2018, *Nature*, **555**, 629

This paper has been typeset from a $\text{\TeX}/\text{\LaTeX}$ file prepared by the author.